SMC-TR-95-31

AEROSPACE REPORT NO.
TR-95(5231)-4

Can the Total Ozone Mapping Spectrometer (TOMS) Measure Ozone Depletion in Rocket Plumes

1 June 1995

Prepared by

J. A. SYAGE
Mechanics and Materials Technology Center
Technology Operations

Prepared for

SPACE AND MISSILE SYSTEMS CENTER
AIR FORCE MATERIEL COMMAND
2430 E. El Segundo Boulevard
Los Angeles Air Force Base, CA 90245

Engineering and Technology Group

THE AEROSPACE CORPORATION
Segundo, California

This report was submitted by The Aerospace Corporation, El Segundo, CA 90245-4691, under Contract No. F04701-93-C-0094 with the Space and Missile Systems Center, 2430 E. El Segundo Blvd., Suite 6037, Los Angeles AFB, CA 90245-4687. It was reviewed and approved for The Aerospace Corporation by S. Feuerstein, Principal Director, Mechanics and Materials Technology Center.

This report has been reviewed by the Public Affairs Office (PAS) and is releasable to the National Technical Information Service (NTIS). At NTIS, it will be available to the general public, including foreign nationals.

This technical report has been reviewed and is approved for publication. Publication of this report does not constitute Air Force approval of the report's findings or conclusions. It is published only for the exchange and stimulation of ideas.

JOHN R. EDWARDS, SMC/CEV
Chief, Environmental Management Division

REPORT DOCUMENTATION PAGE

Form Approved
OMB No. 0704-0188

1. AGENCY USE ONLY (*Leave blank*)	2. REPORT DATE	3. REPORT TYPE AND DATES COVERED
	1 June 1995	

4. TITLE AND SUBTITLE
Can the Total Ozone Mapping Spectrometer (TOMS) Measure Ozone Depletion in Rocket Plumes

5. FUNDING NUMBERS
F04701-93-C-0094

6. AUTHOR(S)
Syage, Jack A.

7. PERFORMING ORGANIZATION NAME(S) AND ADDRESS(ES)
The Aerospace Corporation
Technology Operations
El Segundo, CA 90245-4691

8. PERFORMING ORGANIZATION REPORT NUMBER
TR-95(5231)-4

9. SPONSORING/MONITORING AGENCY NAME(S) AND ADDRESS(ES)
Space and Missile Systems Center
Air Force Materiel Command
2430 E. El Segundo Blvd.
Los Angeles Air Force Base, CA 90245

10. SPONSORING/MONITORING AGENCY REPORT NUMBER
SMC-TR-95-31

11. SUPPLEMENTARY NOTES

12a. DISTRIBUTION/AVAILABILITY STATEMENT
Approved for public release; distribution unlimited

12b. DISTRIBUTION CODE

13. ABSTRACT (*Maximum 200 words*)

The question whether the total ozone mapping spectrometer (TOMS) is capable of measuring ozone levels in a rocket plume is examined. Simulated measurements were computed for four plume scenarios corresponding to 20 and 30 km altitude and 10^3 and 10^4 s elapsed time. For each scenario, we considered plume constituents consisting of the chemical species calculated by Brady and Martin, and three different particle size distributions. For comparison, we also made simulated measurements of ozone total in the absence of particles and in the absence of particles and plume species. Plume measurements by TOMS suffer from two main problems: the detection field of view is typically larger than the column area for ozone loss, and the plume constituents distort the ozone measurement. Another issue limiting sensitivity is that TOMS measures attenuation of solar radiation transmitted through and then backscattered out of the atmosphere; however, only one of these two paths is likely to cross with the plume, unless TOMS is exactly aligned with the plume and the sun. Our simulated TOMS measurements indicate that large errors are caused by interfering absorptions by plume constituents; however, the error decreases to acceptable levels at 10^4 s. Though the large field of view is unfavorable for quantitative measurements, TOMS may be able to obtain evidence of ozone loss in plumes under the following conditions: (1) at times just before the ozone hole recovers when the plume and hole width are greatest, (2) at viewing angles similar to the plume track angle (i.e., maximize viewing pathlength through plume), and (3) at a higher altitude part of the plume (kinetic models indicate that the ozone hole is broader at 30 km than at 20 km).

14. SUBJECT TERMS		15. NUMBER OF PAGES
Ozone Depletion	Rocket Plumes	27
Remote Detection	TOMS	16. PRICE CODE

17. SECURITY CLASSIFICATION OF REPORT	18. SECURITY CLASSIFICATION OF THIS PAGE	19. SECURITY CLASSIFICATION OF ABSTRACT	20. LIMITATION OF ABSTRACT
Unclassified	Unclassified	Unclassified	

Acknowledgments

I benefited from extensive discussions with several people, including Brian Brady and Bob Martin on chemical kinetics modeling of the plume, Ed Beiting on particle size distributions, and Marty Ross on remote passive detection.

Contents

Figures

Tables

1. Introduction

In 1990, Prather and collaborators published a comprehensive study of the Space Shuttle's impact on the stratosphere [*Prather et al.,* 1990a] that has generated a considerable amount of discussion [*Aftergood,* 1991; *McPeters et al.*, 1991]. They investigated the long-term effects using two-dimensional models with complete chemistry [*Ko et al.*, 1989; *Douglass et al.,* 1989] and a three-dimensional model for chemical tracers [*Prather et al.*, 1990b]. From these models, they concluded that at current launch rates, solid rocket motor exhaust does not impose a significant global impact on stratospheric chemistry. An attempt was also made to examine the transient chemical behavior and local impact using a chemical tracer model. These results followed the plume chemistry and dispersion from two days on out to one month. Although these investigators admitted that the early stage of the launch is not adequately modeled, they argued that strict limits can be placed on the ozone impact and that a local column ozone hole cannot occur. This conclusion is based on the following arguments: (1) the chlorine is released predominantly as HCl, which requires considerable time to be converted to active forms of chlorine; (2) the exhaust plume passing through the stratosphere is not aligned vertically; and (3) the exhaust gases can disperse over a 1000 km range in a day.

In 1991 Aftergood [1991] commented on these conclusions raising two important points: a Titan III fly-through observed a 40% reduction in the ambient ozone level [*Pergament,* 1977] although he noted that this measurement is of uncertain reliability; and chlorine is not necessarily exhausted predominantly as HCl, but may contain large quantities of Cl_2 as predicted by an early plume model by Hoshizaki [1975]. Since the comment by Aftergood, a few more facts are known: (1) further modeling evidence of plume afterburning to produce Cl_2 has been reported by Zittel [1992], Denison *et al.* [1994], and Karol [1991]; and (2) the dispersion of the exhaust gas on the timescale of a day may be less extensive than previously postulated [*Prather et al.*, 1990a] according to plume atmosphere transport models [*Ross et al.,* 1994; *Watson et al.,* 1978].

Prather and collaborators rebutted the comment by Aftergood [1991] by citing total ozone mapping spectrometer (TOMS) results [*McPeters et al.,* 1991]. TOMS has a pixel size resolution of 40×40 km^2, which would limit the ability to accurately measure a local ozone hole. However, because the ozone measurement precision of TOMS is a few percent, a significant hole of small extent should be observable. By way of example, Prather explains that a 40% column reduction over a 20×20 km^2 area would appear as a 10% reduction for a single pixel, which is much greater than the detection limit of the TOMS instrument. The TOMS images of several Shuttle trajectories, ranging from about one hour to one day after passage, give no indication of a transient ozone depletion. Ross, however, has argued that the resolution limitations of TOMS would make it difficult to observe a plume ozone depletion [*Ross*, 1992].

The current concensus on the possibility of ozone depletion in rocket plumes is summed up by the World Meterological Organization report [*WMO*, 1991] and more

recently by a Technical Interchange Meeting [*TIM*, 1994]. The evidence presented in the former report does not support a significant global impact; however, it is reported that the role of heterogeneous chemistry is not sufficiently well understood to make a definitive conclusion. TOMS measurements are cited as unsupportive of a local ozone depletion, although spatial resolution limitations are acknowledged. It has since been noted by Ross that the choice of TOMS images presented by McPeters *et al.* [1991] may not have captured the plume track because of the unknown extent of displacement by stratospheric winds [*TIM*, 1994].

Given the above considerations, a number of new questions arise: (1) if TOMS were in proper position, could it detect an ozone hole, and (2) how are ozone measurements perturbed by plume species? We present a quantitative assessment of these issues. The major concern that we address is how other plume constituents affect TOMS ozone measurements. In particular, chlorine oxide compounds in the plume can absorb light in the same spectral region as ozone. TOMS relies on the change in absorption with wavelength to obtain ozone column totals and spatial profiling. The unanticipated presence of plume species that absorb light similarly to ozone can cause an overstatement of the true ozone level. We identified this problem for lidar measurements and suggested methods to minimize the problem [*Syage,* 1994]. This issue was also treated in great detail by Beiting [1994a, 1994b] for *in-situ* ultraviolet absorption measurements, and is being incorporated into the analysis algorithms for interpreting High Resolution Ozone Imaging (HIROIG) measurements [*McKenzie et al.*, 1993].

Another plume property that can lead to measurement error if not properly treated is the attenuation of light due to scattering by alumina particles in the plume. TOMS has only rudimentary provisions for dealing with particle scattering. We examine this issue more thoroughly in Section 4. The analysis presented here regarding the adequacy of TOMS for measuring plume species is based on a modification of a model first used to evaluate direct absorption spectroscopy of a plume using a line-of-sight light source such as solar or stellar irradiation [*Syage,* 1995]. The model is also adaptable for simulating lidar measurements.

2. Background

The TOMS and solar backscattered ultraviolet (SBUV) spectrometer on board the Nimbus 7 spacecraft and the TOMS on Meteor 3 are remote, passive downward-looking absorption spectrometers. The two TOMS instruments are now dead; however, previously recorded images are still being processed. The SBUV spectrometer measures solar radiation backscattered from the Earth's atmosphere at 12 fixed wavelengths in the range of 255.6 to 339.8 nm. It can also operate in a continuous scan mode from 160 to 400 nm in 0.2 nm increments. The TOMS instrument collects atmospheric backscattered radiation in six fixed wavelength channels. Four channels at 312.5, 317.5, 331.2, and 339.8 nm are used to determine total ozone column content. Two channels at 360 and 380 nm are used to determine ground and cloud reflectivity. TOMS provides a crosswise sweep of 35 positions every 8 s. Global coverage is obtained by merging these scans with those from adjacent orbital tracks.

The concept of TOMS is rather straightforward. The instrument measures the directional albedo of the Earth's atmosphere at each wavelength. Using the notation of Herman *et al.*, we define this property as

$$A(\lambda)=\frac{I(\lambda)}{F_0(\lambda)} \tag{1}$$

where $I(\lambda)$ and $F_0(\lambda)$ are the true backscattered radiance and solar irradiance, respectively, and are related to the instrument measured values by the following expression:

$$\begin{aligned} I_m(\lambda) &= I(\lambda)S(\lambda) \\ F_m(\lambda) &= F_0(\lambda)D(\lambda)S(\lambda) \end{aligned} \tag{2}$$

where $S(\lambda)$ and $D(\lambda)$ are the spectrometer sensitivity and diffuser reflectivity, respectively, relative to their initial calibrated values. The diffuser is a plate that is extended periodically to measure solar irradiance and to calibrate the spectrometer. To minimize calibration errors and wavelength independent effects, TOMS reports ratios of albedo for wavelength pairs, the values being defined as $N_p = -100\log_{10}[A(\lambda_1)/A(\lambda_2)]$. The wavelength pairs that are used are summarized in Table I. Atmospheric ozone content is determined by comparing the measured directional albedo ratios to computed tables representing inverse solutions of a multiple scattering (Rayleigh) radiative transfer equation [*Klenk*, 1982]. These tables depend on total ozone Ω, ozone latitude dependence, solar zenith angle Θ, atmospheric pressure at scattering altitudes, and other climatology conditions. A typical set of data are represented graphically as a function of Ω in Figure 1 for a value of $\Theta = 0^\circ$. The sensitivity for measuring total ozone for a particular wavelength pair is proportional to the slope of the N_p vs Ω curve. These curves vary significantly with Θ, resulting in certain pairs being adequate only for limited viewing conditions (see Section 4.5).

Table I. TOMS and SBUV wavelength pairs (adapted from Herman et al. 1991).

Pair (nm)	Designation	Separation (nm)	Sensitivity radiative trans.[b]	$\Delta N_p/\Delta\Omega$ [a] This model[c]
TOMS wavelength pairs				
312.5 / 331.2	A	18.8	0.125	0.168
317.5 / 331.2	B	13.8	0.063	0.080
331.2 / 339.8	C	8.5	0.010	0.011
312.5 / 317.5	A'	5.0	0.062	
317.5 / 339.8	B'	22.3	0.073	0.088
SBUV wavelength pairs				
305.8 / 312.5	D	6.7	0.190	
301.9 / 312.5	E	10.6	0.318	
308.6 / 312.5	D'	4.0	0.103	

[a] $N_p = -100 \log_{10}[A(\lambda_1)/A(\lambda_2)]$, and the ozone column total Ω is in Dobson units (DU), where 1000 DU = 1 atm-cm. $\Delta N_p/\Delta\Omega$ values are for the range 325-375 DU and for vertical solar zenith and viewing angle.

[b] From radiative transfer calculations [*Herman et al.*, 1991].

[c] From single-scattering radiation model used in this report.

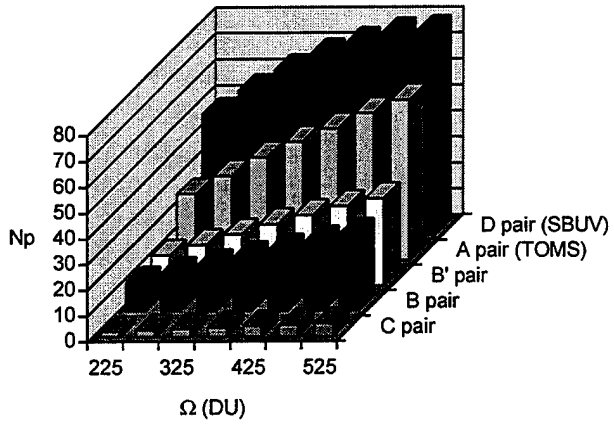

Figure 1.
The dependence of the albedo ratio N_p vs total ozone Ω (mid latitude) for the SBUV D wavelength pair and the four TOMS wavelengths pairs. Data correspond to solar zenith of $\Theta = 0^\circ$, lower boundary reflectivity of R = 0.3. Data are from Herman *et al.*[1991].

An important calibration requirement for TOMS and SBUV is to know the solar irradiance spectrum. This is obtained by measuring the reflection from a diffuser plate at a specific point in the orbit. The ground alumina plate acts as a Lambertian surface having high reflectivity and uniform dispersion and is positioned at appropriate times in front of the spectrometer entrance slit. The diffuser plate is stored in a location that protects it from continual solar radiation, but it apparently is subject to spacecraft outgassing. The cumulative effect of radiation and outgassed material has caused a significant degradation of the diffuser plate reflectivity, which has resulted in an overestimation of actual ozone

levels of about 6% by TOMS on Nimbus 7. Among the upgrades on the Meteor 3 TOMS is a new diffuser plate configuration. However, since nearly all reported ozone profiles, including the images that appears in McPeters et al. [1991], are from the Nimbus 7 TOMS, a brief description of instrumental problems is in order.

An elaborate effort was undertaken to estimate the change in diffuser reflectivity, and a correction algorithm has been developed to adjust the measured ozone levels. Even more perplexing is that although the SBUV measured solar flux decreases almost linearly with time, the TOMS measured solar flux decreases in a much more complicated manner, indicating that the instrument sensitivity may also be changing with time. Other problems plague ozone measurements. (1) A small synchronization timing error has developed between passage of the slits in front of the spectrometer entrance aperture and the photon counting electronics. (2) An error has developed in determining the spacecraft roll, pitch, and yaw angles. (3) Different wavelength pair measurements yield a 1-4% disagreement in calculated total ozone, and there is a 3% disagreement between TOMS and SBUV. These errors are inexplicable, but may be due to the initial instrument calibration. (4) Sea glint in the 360 and 380 nm channel and a slow longitudinal drift in the Nimbus 7 orbit has introduced error in ozone measurements, which must now be corrected. Although each of these problems has a correction algorithm, the uncertainty in making total ozone measurements accumulates. Fully corrected data are typically reported to an accuracy of 1-2%; however, each of these errors cited above contributes a few percent uncertainty if uncorrected. We will ignore these problems for now and assume that the TOMS spectrometer performs to design specifications.

The current TOMS data analysis assumes that the backscattered radiance $I(\lambda)$ is attenuated by ozone absorption and Rayleigh scattering. Methods have been developed to deal with the effect of aerosols on the estimation of total column ozone [*Dave*, 1978; *Torres et al.,* 1992; *Bhartia et al.,* 1993], but not for the case of a dense alumina-laden plume. Nor are absorbing species considered other than that which exists in the ambient atmosphere. Below, we consider how the measured value of $I(\lambda)$ is affected by the presence of plume constituents. Since we cannot carry out a full radiative transfer calculation, we instead use a simpler single scattering expression to calculate how the detected backscattered radiance is modified by the presence of the plume species and how it affects the estimation of the total ozone column. This simpler approach is valid because we are working with a model atmosphere and calculating how well TOMS measures *changes* in ozone levels in the presence of plume species.

3. Model of Scattered Radiation

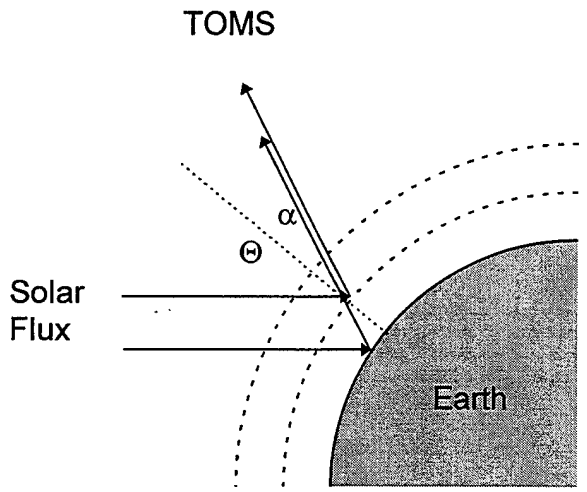

Figure 2.
Solar transmission through atmosphere and backscatter radiation in direction of TOMS (viewing angle α). Dotted lines represent different layers of the atmosphere. The distribution of scattering depth varies with wavelength and solar zenith angle Θ. Scattering of incident light off of plume particles is not shown in this picture.

The relationship between solar irradiance and detected scattered radiance by TOMS is diagrammed in Figure 2. The transmission of solar irradiance through the atmosphere depends strongly on wavelength, primarily due to absorption by ozone. Long wavelength light, which is weakly absorbed, penetrates much deeper than short wavelength light (e.g., < 300 nm), which is strongly absorbed by ozone. One can define a scattering depth profile or effective scattering level that relates the distribution of altitude from Earth from which photons are scattered back to space. The analysis of species content by absorption of backscattered radiance is simplified if the radiance at particular wavelengths originates from well-defined scattering layers. The scattering distribution at 312.5 nm peaks at about 5-10 km altitude (depending on solar zenith angle, among other things), which is well below the ozone distribution. This partly explains the choice of TOMS detection wavelength in Table I. By comparison, the effective scattering distribution for 292 nm peaks at about 40-50 km.

We begin with a model for detecting scattered radiation by TOMS that incorporates an integration over the distribution of scattering levels for particular wavelengths and that includes attenuation of backscattered signal by plume species, including alumina particles. The governing equation is given by

$$I(\lambda) = \Gamma(\alpha,\lambda)\int_0^\infty I_0(\lambda,s) \times \exp\left\{-p(\alpha)\left[\tau_R(\lambda,s)+\tau_{O_3}(\lambda,s)\right]+p(\alpha,\varphi)\sum_i \tau_i(\lambda,s)\right\} ds \qquad (3)$$

where the intensity of backscattered light originating from altitude s is given by

$$I_0(\lambda,s) = F_0(\lambda)\sigma_R(\lambda)n_R(s)\Psi(\Theta,\alpha,\lambda) \times \exp\left\{-p(\Theta)\left[\tau_R(\lambda,s)+\tau_{O_3}(\lambda,s)\right]\right. \quad (4)$$

and the attenuation terms are given by

$$\tau_R(\lambda,s) = \sigma_R(\lambda)\int_0^{r_0} dr \int_s^{\infty} ds' n_R(r,s')$$

$$\tau_{O_3}(\lambda,s) = \sigma_{O_3}(\lambda)\int_0^{r_0} dr \int_s^{\infty} ds' n_{O_3}(r,s') \quad (5)$$

$$\tau_i(\lambda,s) = \sigma_i(\lambda)\int_0^{r_0} dr \int_s^{\infty} ds' n_i(r,s')$$

Other parameters are defined as follows:

- Θ - Solar zenith angle (see Figure 2),
- α - TOMS viewing angle (see Figure 2),
- φ - plume track angle,
- $I(\lambda,r)$ - backscattered radiance,
- $F_0(\lambda)$ - incident irradiance,
- $\Gamma(\alpha,\lambda)$ - spectrometer response function and collection efficiency,
- σ - attenuation cross sections, where subscripts are: R=Rayleigh scattering, O_3=ozone, i=plume species,
- $n(r,s)$ - molecular or particle density, where subscripts are defined above,
- $\Psi(\alpha,\Theta,\lambda)$ - Rayleigh phase function at scattering angle $\alpha+\Theta$,
- $p(\Theta)$, $p(\alpha)$ - pathlength factor for transmitted and backscattered radiation, given by secΘ and secα, respectively,
- $p(\alpha,\varphi)$ - pathlength factor through the plume, which is dependent on plume track angle φ, as described later,
- s, s_0 - vertical distance from the Earth's surface and altitude of assumed scattering layer, respectively (see Figure 3),
- r, r_0 - radial distance from center point of TOMS pixel and radius of pixel resolution, respectively (see Figure 3).

The ozone depletion in the plume is included in the sum of plume species and is represented by a negative density relative to the ambient ozone density. The analysis simplifies considerably if one assumes that all backscatter originates from a narrow effective scattering layer below the ozone layer and plume track, in which case the integral over s' can be replaced by a constant. Equations (3)-(5) can then be rewritten as

$$I(\lambda) = \kappa(\Theta,\alpha,\lambda)\exp\left\{-\left[p(\Theta)+p(\alpha)\right]\left[\tau_R(\lambda)+\tau_{O_3}(\lambda)\right]- p(\alpha,\varphi)\sum_i \tau_i(\lambda)\right\} \quad (6)$$

where

$$\begin{aligned}
\tau_R(\lambda) &= \sigma_R(\lambda)\int_{s_0}^{\infty} ds\; n_R(s) \;=\; \sigma_R(\lambda)\overline{N}_R \\
\tau_{O_3}(\lambda) &= \sigma_{O_3}(\lambda)\int_{s_0}^{\infty} ds\; n_{O_3}(s) \;=\; \sigma_{O_3}(\lambda)\overline{N}_{O_3} \\
\tau_i(\lambda) &= \sigma_i(\lambda)\int_0^{r_0} dr \int_{s_0}^{\infty} ds\; n_i(r,s) = \sigma_i(\lambda)\int_0^{r_0} dr\, N_i(r) = \sigma_i(\lambda)\overline{N}_i
\end{aligned} \quad (7)$$

and where $\kappa(\Theta,\alpha,\lambda)$ is a constant that includes the irradiance, scattering functions, instrument functions, and any other factors that are invariant to the plume properties; the τ terms are attenuation factors; the N terms are peak column numbers through the center of the plume; and the $\overline{N}$ terms are average column numbers over the TOMS pixel resolution. The calculated attenuation due to particle scattering may be overestimated (by as much as 50%) because the scattering tends to be in the forward direction and not isotropic. We define the spatial distribution functions for r and s as $f(r)$ and $g(s)$, respectively. We assume that Rayleigh scattering is due to air and $g_R(s)$ is reasonably described by an exponential. The n_R and n_{O3} distributions of the ambient atmosphere are treated as uniform in the horizontal r dimension. The ambient ozone vertical distribution is fitted to a Gaussian distribution. Gaussian distributions based on the plume widths are used to describe the horizontal and vertical distributions for the O_3 hole and for the plume species i. The Gaussian widths we use along the axial s and radial r dimensions are explained in the following section. Ross [1994] has computed three-dimensional (3D) spatial profiles for ozone and finds that the results vary greatly with wind flow fields and launch vectors. In general, ozone depletion peaks near the center and falls off fairly uniformly with distance. Given the variability of these distributions, it seems reasonable to assume Gaussian distributions as a representative case. This approach is justifiable since the average of all events is representative of a single event, in which case a Gaussian distribution is a good model for the average situation. However, it may be useful to do the present analysis for specific 3D spatial profiles to test the sensitivity of TOMS measurements to these variations.

4. Results and Discussion

We begin by defining a physical model of the plume and presenting relevant data and information. We rely on the kinetic modeling calculations by Brady and Martin for the species concentrations with time and also for defining the spatial and temporal scales over which ozone depletion occurs. Species concentrations and absorption cross sections are tabulated in Appendices A and B.

4.1. Plume dispersion and displacement

Plume flow dynamics is a complex phenomenon. For the purposes of the present discussion, a simple model will suffice. Figure 3 illustrates the relationship of plume dynamics relative to the TOMS detection line-of-sight. We refer to Watson *et al.* [1978] for information on stratospheric plume dynamics. There are two principal trends in stratospheric dispersion. First, air flow in the stratosphere occurs almost entirely in horizontal planes (shearing). Horizontal motion consists of displacement by circulatory advection and dispersion by eddy diffusion. In the stratosphere, horizontal velocities (about 1-100 m/s) greatly exceed vertical velocities (0.0001-0.10 m/s). Second, the rate of dispersion increases with increasing spatial scales. The movement of air parcels is more correlated over small scales than over large scales. Watson *et al.* [1978] modeled Shuttle plume dispersion in the stratosphere and found that the horizontal plume width followed a 1.4 power dependence with time over a period of several seconds to several days. Recently, Beiting [1995] analyzed a plume video and noticed that the expansion over the first 10 min is much greater than predicted by the Watson dependence. Plume dispersion is an important issue to the chemistry of ozone depletion and to the observation of plume composition. Further studies of plume expansion over longer times are essential. Until then, we will use the Watson dispersion model in order to be consistent with the chemical modeling used in this analysis.

4.2. Time scales

Using the Watson dispersion rate, Brady and Martin [1994] computed plume widths of 10 km (20 km altitude) and 28 km (30 km altitude) at a time of 10^4 s when ozone depletion begins to recover (see Appendix A). Their kinetic models indicate that ozone depletion due to plume chemistry persists for about 10 h before returning to near ambient levels. The maximum extent of the hole is about 30 km for the upper stratosphere. We restrict our calculations to times less than 10 h.

4.3. Plume distributions

It is unclear how the density of plume species varies across the plume width. Brady and Martin calculate densities along the centerline only. However, these densities conserve total chlorine across the plume width, which implicitly assumes a uniform density across the plume. We expect the initial mixing of the exhaust plume with air and subsequent

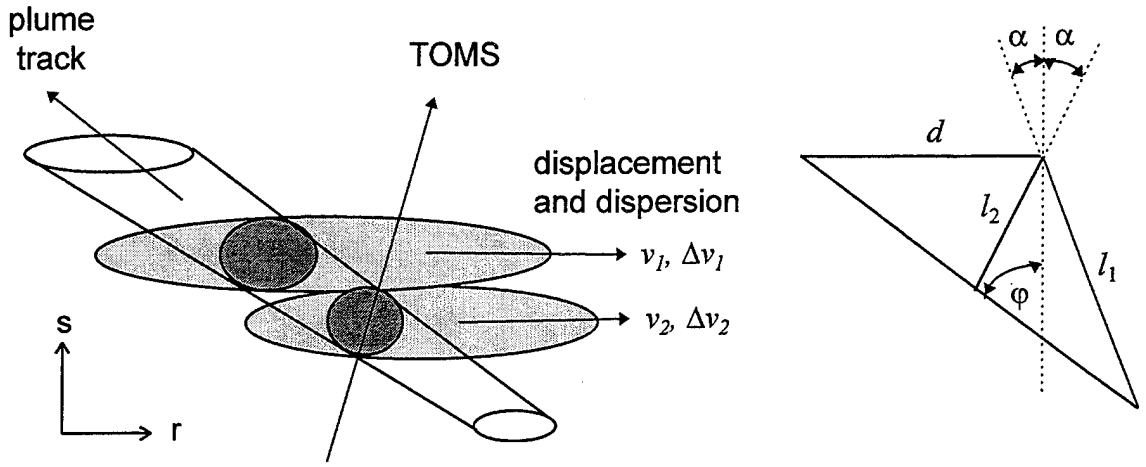

Figure 3.
Diagram of the plume track and TOMS viewing angle. Representative air parcels at early time (dark shade) and later time (light shade) schematically show horizontal displacement and dispersion. The plume track is shown to increase in width at higher altitudes due to the lower atmospheric pressure against which the exhaust expands. The pathlength along the TOMS line-of-sight l is proportional to the horizontal plume diameter d by a factor that depends on the viewing angle α and the plume track angle φ. Two different viewing angles are diagrammed on the right. The angle φ can change with time and altitude due to differential wind velocities as a function of altitude.

dispersion to give a Gaussian-like distribution of species off centerline (or perhaps a flat-top Gaussian). We, therefore, renormalize the Brady and Martin uniform concentrations to fit a Gaussian distribution (i.e., the square-shaped distribution is replaced by a Gaussian distribution of equivalent area). Other functional forms can be handled by our treatment; the exact form is not important for TOMS monitoring because the pixel resolution is greater than the maximum ozone hole. However, we choose to set up the problem with some reasonable density distribution in order to have the mechanics available to consider different distributions and to model the signal collected by higher resolution instruments (e.g., HIROIG and lidar).

The picture in Figure 3 is intended to show the rudiments of displacement and dispersion with time. Also,we note that differential velocities with altitude can distort the plume vector. All of these issues make it difficult to estimate a TOMS pathlength through the plume. A rigorous treatment would take computed spatial distributions in the spirit of Ross [1994] and integrate over the TOMS field-of-view. However, lacking this information and noting that the spatial distributions of plume species are extremely sensitive to wind conditions and launch vectors, no specific situation is representative; so perhaps a simple model is no less representative.

As a working approximation, we assume an initial plume diameter of 0.20 km (see Appendix A, 20 km altitude); a plume track angle of $\varphi=50^\circ$; and a TOMS viewing angle of $\alpha=0^\circ$. This leads to a horizontal plume width of d = 0.15 km and a TOMS pathlength

through the plume of $l = 0.13$ km. After 10^3 s, the plume horizontal width has expanded to about 7.0 km, yielding a TOMS pathlength of 5.9 km, assuming that the plume axis remains constant (i.e., differential drift and dispersion are negligible). The length of the plume track through the stratosphere is about 20 km. This simple picture assumes that plume parcels from above and below drift into view relative to the early time viewing volume (see Figure 3). However, these different parcels have different dispersion and displacement rates which complicates the analysis. To simplify analysis, we target an initial volume at some particular altitude and simulate the vertical pathlength by a Gaussian distribution of width l, where the peak is given by the calculated species densities for a particular time and altitude. Examples of vertical distributions for lines-of-sight intersecting the plume centerline at different altitudes are given in Figure 4. Since we assume that the density profile in the horizontal profile is also Gaussian, the vertical distributions away from the plume centerline will show narrower and less intense density profiles than those in Figure 4. This would best be seen using contour plots looking down a vertical axis.

4.4. Simulated ozone measurements

The total vertical column for ambient ozone in this example is 375 DU (0.375 atm-cm). In the vicinity of a plume at 20 km, the model predicts an ozone column depletion of 22 and 73 DU at 10^3 and 10^4 s, respectively. These column totals and the horizontal dispersion are consistent with results by Ross (1994). At 30 km, the predicted ozone column depletion is 58 and 191 DU at 10^3 and 10^4 s. These values considerably exceed those calculated by Ross. However, it should be noted that the Brady and Martin model is not directly comparable to the Ross model because the former calculates centerline concentrations only, whereas the latter calculates spatial extent.

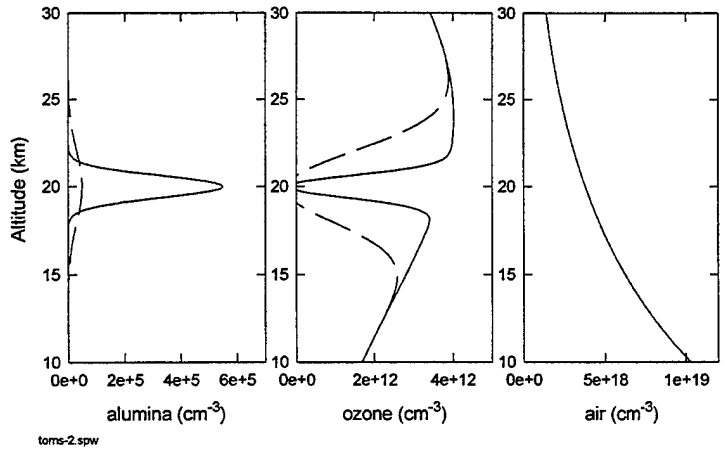

Figure 4.
Vertical density profiles through the center of the plume at 20 km altitude and 10^3 s (solid line) and 10^4 s (dashed line) elapsed time. Alumina particle size is assumed to be 0.1 μm (Model I, Appendix A). The increased vertical thickness at later times is due to the drift of adjacent air parcels, as diagrammed in Figure 3.

Table II. Simulated TOMS measurement of ozone column depletion (DU units) at different plume altitudes and elapsed time.

Wavelength Pair	Plume Model[a]				
	I	II	III	IV	V
	20 km, 10^3 s, $\Delta\Omega = -23$ DU[b]				
A	-10.0	-13.4	-12.8	-12.8	-0.25
B'	0.5	-7.0	-5.7	-5.8	-0.25
B	-13.5	-16.0	-14.9	-15.0	-0.25
C	120	71	74	74	-0.25
	20 km, 10^4 s, $\Delta\Omega = -76$ DU[b]				
A	-0.6	-3.9	-3.4	-3.4	-3.0
B'	3.2	-4.3	-3.1	-3.1	-3.0
B	-2.0	-4.5	-3.4	-3.5	-3.0
C	47	-2.8	0.4	0.2	-3.0
	30km, 10^3 s, $\Delta\Omega = -58$ DU[b]				
A	0.6	-12.4	-12.1	-12.1	-1.9
B'	-2.9	-7.1	-6.4	-6.4	-1.9
B	-13.1	-14.6	-14.0	-14.0	-1.9
C	81	57	59	59	-1.9
	30 km, 10^4 s, $\Delta\Omega = -191$ DU[b]				
A	-16.5	-18.3	-18.0	-18.0	-21.1
B'	-14.6	-18.8	-18.1	-18.1	-21.1
B	-17.5	-19.0	-18.4	-18.4	-21.1
C	11.0	-17.0	-15.8	-15.4	-21.1

[a] Model I - plume molecules and 0.1 μm particles,
II - plume molecules and 1.0 μm particles,
III - plume molecules and trimodal particle distribution,
IV - plume molecules and no particles,
V - no plume molecules and no particles.

[b] True vertical column depletion at the center of the plume. For comparision, $\Omega = 375$ DU for the undisturbed atmosphere in our calculation.

The ability to measure ozone depletions by TOMS depends strongly on plume constituents. Table II summarizes the various models of plume constituents used to simulate measurements of ozone depletion. Simulated TOMS measurements of ozone depletion for four test cases (20 and 30 km plume altitude, 10^3 and 10^4 s lapse time) were conducted. Results for a vertical line-of-sight, $\alpha=0^\circ$, are summarized in Table II and in Figure 5. From Table II it is evident that the measured ozone depletion varies significantly

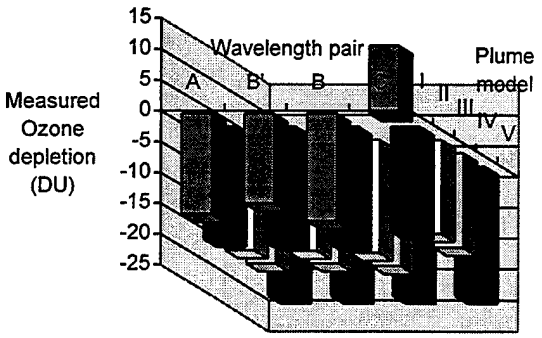

Figure 5.
Graphical representation of Table II results for 30 km, 10^4 s plume. The 0.1μm particle sizes assumed in Model I give erroneous ozone readings. The C pair is a much less reliable measure of ozone than the other pairs. The correct ozone deficit is -191 DU.

depending on plume conditions. The following points constitute the major trends and observations:

1. For small plume diameters, which occur at early times, the measured change in ozone total $\Delta\Omega$ understates the true ozone change due to the averaging of a small column width over the TOMS pixel resolution of 40 km square.
2. At early times, the TOMS ozone measurement is severely distorted because of the high density of plume species that have overlapping absorptions with ozone. Ironically, the distorted readings in Table II (Models I-IV) give results that are closer to the actual ozone depletion than the readings for the ideal case (Model V).
    - This is a false ozone depletion caused by the relatively high density of Cl_2 (see Appendix A), which has a differential absorption for the A, B, and B' wavelength pairs that is opposite to that of ozone (see Appendix B). That is, it looks like "anti-ozone" and, therefore, exaggerates the ozone loss. For the C pair, Cl_2 has a differential absorption similar to ozone and, therefore, looks like ozone, thus exaggerating the amount of ozone.
    - ClO has a differential absorption similar to ozone and therefore causes an understimate of the ozone loss. This effect is not large, but is evident for the case of the 30 km high plume after 10^4 s (compare Models I-IV to Model V).
3. TOMS measurement accuracy increases with increasing elapsed time because the ozone hole width increases to fill a greater fraction of the TOMS pixel. The total Cl_2 content also decreases with time (other chlorine compounds increase in relative concentration), thus decreasing the measurement distortion. The results in Table II indicate that TOMS should be capable of detecting an ozone depletion in the region where the plume track is at 30 km and has expanded for 10^4 s.
4. Ozone determinations from the C pair are inherently inaccurate because of the small absorption cross sections for ozone relative to the other species at these wavelengths.

5. The most accurate measurements of ozone depletion are made by the A pair at long times. The best time to measure is just before the ozone hole recovers, when the plume width is largest.

6. The variation of measured ozone depletion for Models I to III correspond to sensitivity to different particle size distributions. Of these distributions, the largest inaccuracies occur for the 0.1 μm particle case (Model I). This is explained by the size being similar to the wavelength of light, which accounts for a large scattering cross section.

As a final test, we examine the effect of varying the viewing angle with respect to the plume track angle. Qualitatively, we expect the smallest plume pathlength when viewing perpendicularly. The effective pathlength can become quite large when viewing nearly parallel to the plume track, as portrayed in the geometric sketch in Figure 3. Figure 6 shows measured column ozone depletions as a function of viewing angle α. The example given is for a 20 km altitude plume after 10^4 s and has a computed peak vertical column depletion of -76 DU (see Table II). At TOMS viewing angles of $\alpha = 0^\circ$ and 40° relative to the plume track angle of $\varphi = -50^\circ$, the ozone depletion readings are -5.9 and -3.9 DU, respectively, which are probably too small to be detected by TOMS. However, at a viewing angle of $\alpha = -40^\circ$, nearly parallel to the plume track, a TOMS ozone depletion reading of -20.2 DU is obtained, which may be detectable. Except for the C pair results, the measured ozone losses in Figure 6 are fairly consistent for different wavelength pairs and models of plume species.

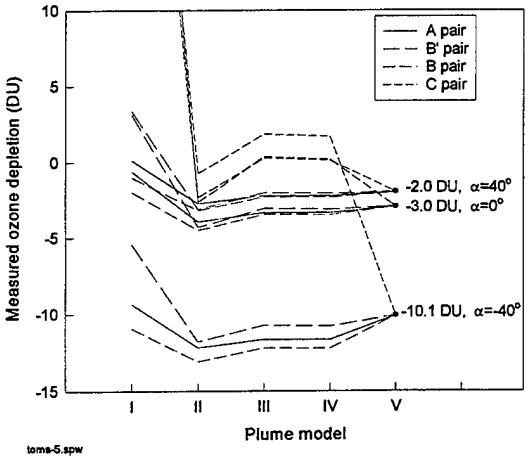

Figure 6.
Simulated ozone loss measurement for different TOMS viewing angles α. The example given is for a 30 km high plume after 10^4 s. The $\alpha=0^\circ$ results are given in Table II, as is the description of the plume composition Models I-V.

If this analysis indicates that TOMS is capable of measuring an ozone depletion under favorable circumstances, then why wasn't a depletion evident in the TOMS images presented by McPeters et al. [1991]? According to Ross [*TIM*, 1994] the plume track was considerably displaced by winds from where the pictures were taken; hence, the images did not actually capture the plume. Perhaps a search of other images might reveal an effect. However, actual plume monitoring requires a means to track the plume. After-the-fact searches of TOMS images may not be useful unless the plume displacement is known.

4.5. Signal strength and sensitivity analysis

To gain an appreciation of the sensitivity needed to obtain reliable ozone measurements, we compare in Table III calculated albedo values $A(\lambda)$ for detection of backscattered radiance through a 30 km altitude plume vs an ambient atmosphere. A comparison of the ambient vs Model V shows the change in signal due to the plume ozone hole only. The change is quite modest. The attenuations due to plume species are at least as great as the effect of ozone depletion on detected signal. Even if the plume composition were known exactly and the signal could be corrected for these interfering absorptions, the uncertainty in measuring the individual contributions to the signal would introduce an uncertainty into the overall measure of $I(\lambda)$ and, therefore, of $A(\lambda)$. The latter value also depends on how well $F_0(\lambda)$ is known or can be determined.

As described earlier, ozone content is estimated by TOMS by matching differential absorption measurements for each wavelength pair to a look-up table or function relating values of the albedo ratio N_p to Ω (see Figure 1). In the above analysis, we interpolated ozone content from a grid of calculated N_p. Using the definition of N_p

$$N_p = -100 \cdot \log_{10}\left[\frac{A(\lambda_1)}{A(\lambda_2)}\right] \tag{8}$$

and Eqs. (1), (5), and (6), we can write an expression for sensitivity

$$\begin{aligned}\frac{d\Omega}{dA(\lambda_2)} &= \left\{\frac{dN_p}{dA(\lambda_2)}\right\}\left\{\frac{d\Omega}{dN_p}\right\} \\ &= \frac{43.4}{A(\lambda_2)}\left\{\frac{\Delta\Omega}{\Delta N_p}\right\}\end{aligned} \tag{9}$$

where we have chosen to measure the sensitivity of measured Ω to one of the detected signals in a pair measurement. Over any moderate range of ozone content, $d\Omega/dN_p$ is relatively constant and can be approximated by a constant slope evaluated at some value of Ω (tabulated in Table I). The sensitivity of Ω to measured $A(\lambda_2)$ is then given by

$$\Delta\Omega = 43.4 \frac{\Delta\Omega}{\Delta N_p} \frac{\Delta A(\lambda_2)}{A(\lambda_2)} \tag{10}$$

One readily sees that small percentage uncertainties in $A(\lambda_2)$ can lead to large errors in measuring Ω. The A pair provides the best sensitivity (Table I), such that a 1% measurement uncertainty corresponds to a 10 DU uncertainty in Ω. On the other hand, a 1% measurement uncertainty for the C pair gives a 160 DU ozone uncertainty.

Table III. Computed values of the wavelength dependent albedo $A(\lambda)$.

Wavelength	**Plume Model**[a]					
(nm)	I	II	III	IV	V	ambient
	30 km, 10^3 s					
312.5	0.070	0.072	0.073	0.074	0.099	0.097
317.5	0.153	0.157	0.159	0.160	0.221	0.219
331.2	0.322	0.329	0.334	0.338	0.486	0.486
339.8	0.385	0.388	0.394	0.399	0.559	0.559
	30 km, 10^4 s					
312.5	0.105	0.109	0.110	0.111	0.116	0.097
317.5	0.222	0.228	0.231	0.234	0.239	0.219
331.2	0.462	0.472	0.479	0.484	0.491	0.486
339.8	0.535	0.539	0.548	0.554	0.561	0.559

5. Summary and Conclusions

In this report, we have presented a quantitative analysis of the potential for TOMS to detect ozone depletion in rocket plumes. This study was motivated by a paper by McPeters et al. [1991] indicating that TOMS ozone images provide no evidence of an ozone hole. The spatial resolution of TOMS is acknowledged to be much greater than the reputed ozone hole size; however, when averaged over the TOMS pixel resolution, McPeters et al. argue that an ozone depletion should still be observable. Subsequent to that paper, it was noted by Ross [*TIM*, 1994] that the images did not capture the plume track because of unaccounted for displacement of the plume by stratospheric winds. Hence the question remains, can TOMS detect ozone depletion in a plume when properly positioned? To answer this question, the effect of all plume species on the TOMS differential absorption algorithm must be considered. We use the chemical kinetics results of Brady and Martin and assume representative spatial distributions for the plume species. We also consider several models for particle size distributions and include the wavelength dependent scattering cross sections. The simulated TOMS measurements show that the plume species can alter ozone readings

In addition to the plume absorption interferences, TOMS suffers from other disadvantages that include: (1) pixel resolution diminishes sensitivity to ozone changes on the small spatial dimensions of the plume, (2) the use of only four wavelengths limits the ability to distinguish differential absorptions from species other than ozone, (3) the constraints of an orbiting satellite do not allow it to achieve a favorable position for optimizing plume measurements. New technology is being introduced into the design of remote passive absorption spectrometers to overcome some of these problems. For example, HIROIG is designed to record spectra continuously from 270-370 nm with 2 km horizontal resolution. HIROIG, therefore, can potentially identify interfering absorptions and correct for their presence in determining ozone levels.

Based on our model for TOMS ozone detection and our best estimate of the composition of SRM plumes at various altitudes and elapsed times after rocket passage, we conclude that TOMS is not well suited to detecting plume ozone depletion. Because of insufficient spatial resolution for detecting potential plume ozone depletions, TOMS typically gives readings that are near the instrument intrinsic noise level. A detectable signal may be possible if (1) the solar angle matches the viewing angle, so that the detected backscatter arises from light that undergoes two passes through the plume, (2) TOMS captures the plume at its peak ozone column depletion and width, and (3) the viewing angle is aligned along the plume track to maximize the plume pathlength. These conditions are not typical and exceedingly rare in combination. A detectable signal would still have a significant uncertainty due to the problem of spectral interference from plume species.

References

Archival Publications

Aftergood, S.,"Comment on 'The space shuttle's impact on the stratosphere' by M. J. Prather et al.," *J. Geophys. Res.* **96**, 17,377 (1991).

Bhartia, P. K., J. Herman, R. D. McPeters, and O. Torres, "Effect of Mount Pinatubo aerosols on total ozone measurements from backscatter ultraviolet (BUV) experiments," *J. Geophys. Res.* **98**, 18,547-18,554 (1993).

Dave, J. V., "Effect of aerosols on the estimation of total ozone in an atmospheric column from the measurements of its ultraviolet radiance," *J. Atmos. Sci.* **35**, 899-911 (1978).

DeMore, W. B., S. P. Sander, D. M. Golden, R. F. Hampson, M. J. Kurylo, C. J. Howard, A. R. Ravishankara, C. E. Kolb, and M. J. Molina, "Chemical kinetics and photochemical data for use in stratospheric modeling," Evaluation number 10, JPL Publication 92-20 (August 15, 1992).

Denison, M. R., J. J. Lamb, W. D. Bjorndahl, E. Y. Wong, and P. D. Lohn, "Solid rocket exhaust in the stratosphere: Plume diffusion and chemical reaction," *J. Spacecraft & Rocket*, **31**, 436 (1994).

Dobson, G. M. B., "Forty years' research on atmospheric ozone at Oxford: A history," *Appl. Opt.* **7**, 387 (1968).

Douglass, A. R., C. H. Jackman, and R. S. Stolarski, "Comparison of model results transporting the odd nitrogen family with results transporting separate odd nitrogen species," *J. Geophys. Res.* **94**, 9862-9872 (1989).

Grant, W. B., ed., "Ozone measuring instruments for the stratosphere," Vol. 1 of *Collected Works in Optics* (Optical Society of America, Washington D.C., 1989).

Herman, J. R., R. Hudson, R. McPeters, R. Stolarski, Z. Ahmad, X.-Y. Gu, S. Taylor, and C. Wellemeyer, "A new self-calibration method applied to TOMS and SBUV backscattered ultraviolet data to determine long-term global ozone change," *J. Geophys. Res.* **96**, 7531-7545 (1991).

Hoshizaki, H. (chairman), "Aircraft wake microscale phenomena," in *The Stratosphere Perturbed by Propulsion Effluents, CIAP Monogr.* 3, chap. 2., pp. 60-73, Climatic Impact Assessment Program, U.S. Dept. of Transportation, Washington D. C., Sept. 1975.

Karol, I. L., Y. E. Ozolin, and E. V. Rozanov, "Effect of space rocket launches on ozone and other atmospheric gases," paper presented at the Europea Geophysical Association Conference, Wiesbaden (1991).

Klenk, K. F., P. K. Bhartia, A. J. Fleig, V. G. Kaveeshwar, R. D. McPeters, and P. M. Smith, "Total ozone determination from the backscattered ultraviolet (BUV) experiment," *J. Appl. Meteorol.* **21,** 1672-1684 (1982).

Ko, M. K. W., K. K. Tung, D. K. Weinstein, and N. D. Sze, "The roles of dynamics and chemical processes in determining the stratospheric concentration of ozone in 1-D and 2-D models," *J. Geophys. Res.* **94**, 9889-9896 (1989).

McKenzie, D. L., et al., "System requirements for the high-resolution ozone imager (HIROIG)," The Aerospace Corporation, TR-93(3231)-2 (Sept. 15, 1993).

McPeters, R., M. Prather, and S. Doiron, "Reply," *J. Geophys. Res.* **96**, 17,379 (1991).

Pergament, H. S., R. I. Gomberg, and I. G. Poppoff, "NO_x deposition in the stratosphere from the space shuttle rocket motors," Appendix G to *NASA Tech. Memo.* X-58198, G-3, Jan. 1977.

Prather, M. J., M. M. Garcia, A. R. Douglass, C. H. Jackman, M. K. W. Ko, and N. D. Sze, "The space shuttle's impact on the stratosphere," *J. Geophys. Res.* **95**, 18,583-18,590 (1990a).

Prather, M., M. M. Garcia, R. Suozzzo, and D. Rind, "Global impact of the antarctic ozone hole: Dynamical dilution with a 3-D chemical transport model," *J. Geophys. Res.* **95**, 3449 (1990b).

Ross, M. N. "Potential impact of solid rocket motor exhaust on stratospheric ozone," The Aerospace Corporation, TOR-92(2565)-2 (1992).

Syage, J. A., "Direct absorption spectroscopy of a solid rocket plume" The Aerospace Corporation, TOR-95(5231-16)-1 (April 15, 1995).

Technical Interchange Meeting (TIM), "Launch Vehicles Working Group," NASA HQ, Washington, D.C. (Sept. 15-16, 1994).

Torres, O., Z. Ahmed, and J. R. Herman, "Optical effects of polar stratospheric clouds on the retrieval of TOMS total ozone," *J. Geophys. Res.* **97**, 13,015-13,024 (1992).

Watson, R. T., P. E. Smokler, and W. B. DeMore, "An assessment of an F_2 or N_2O_4 atmospheric injection from an aborted space shuttle mission," JPL Publication 77-81 (April 15, 1978).

World Meterological Organization (WMO), Chapter 10, "Predicted Rocket and Shuttle Effects on Stratospheric Ozone," from the Scientific Assessment of Ozone Depletion: 1991.

Zittel, P. F., "Local effect of large, solid rocket motors on stratospheric ozone," The Aerospace Corporation, ATR-92(9558)-2 (August 10, 1992).

Internal Aerospace Reports

Beiting, E. J., "In-situ stratospheric ultraviolet absorption and extinction measurements in a Titan IV plume," The Aerospace Corporation, ATM-94(4448)-7 (June 20, 1994a).

Beiting, E. J., "In-situ stratospheric measurement of total particle surface area in SRM plumes by optical transmissometer," The Aerospace Corporation, ATM-94(4232-05)-1 (Sept. 9, 1994b).

Beiting, E. J. "Solid rocket motor stratospheric plume dispersion," The Aerospace Corporation, ATM-95(5231-16)-3 (April 20, 1995).

Brady, B. B., and L. R. Martin, "Modeling solid rocket booster exhaust plumes in the stratosphere with SURFACE CHEMKIN," The Aerospace Corporation, ATM-94(4231-16)-2 (Oct. 17, 1994).

Ross, M. N., D. L. McKenzie, and J. H. Hecht, "Ground-based observation of ozone loss in the STS 65 exhaust plume," The Aerospace Corporation, ATM-94(4232-04)-1 (July 1, 1994).

Syage, J. A., "Monitoring of ozone in a solid rocket motor plume by airborne differential absorption lidar (DIAL)," The Aerospace Corporation, ATM-94(4448)-6 (May 26, 1994).

APPENDICES

Appendix A.

Concentrations (cm^{-3}) of plume species along the centerline for a Titan IV launch.

	20 km 10^3 s	20 km 10^4 s	30 km 10^3 s	30 km 10^4 s
O_3	1.7×10^9	5.4×10^9	6.1×10^9	4.3×10^{11}
Cl_2	2.4×10^{14}	9.0×10^{11}	2.5×10^{13}	6.9×10^{10}
ClO	1.3×10^{12}	9.9×10^{10}	2.6×10^{11}	8.1×10^{10}
ClOO	2.1×10^{10}	1.4×10^9	8.8×10^8	6.9×10^5
ClOOCl	2.5×10^9	4.0×10^8	6.4×10^7	1.1×10^{10}
HOCl	2.0×10^8	5.2×10^8	2.6×10^7	3.4×10^8
OClO	8.4×10^7	8.5×10^6	1.4×10^7	5.4×10^7
Model I[a] 0.1μ particle	5.5×10^5	5.0×10^4	3.9×10^4	3.4×10^3
Model II[a] 1.0μm particle	5.5×10^2	50	39	3.4
Model III[b]				
0.056μm particle	4.1×10^4	3.7×10^3	2.9×10^3	2.6×10^2
1.0μm particle	10.3	0.93	0.74	0.06
3.6μm particle	11.2	1.01	0.80	0.07
plume width, d[c]	2.1 km	7.0	5.9	20.0
pathlength, l[d]	1.8 km	5.9	5.0	16.8

[a] Constant particle size.

[b] Sauter mean diameter for log normal distribution, evaluated by Beiting (1994b).

[c] Initial plume width is 0.20 and 0.56 km diam at 20 and 30 km altitude, respectively, calculated from Brady and Martin (1994).

[d] Calculated for plume angle of $\varphi=50^\circ$.

Appendix B.

Absorption cross sections of plume species (units of 10^{-20} cm^2).[a]

	312.5 nm	317.5 nm	331.2 nm	339.8 nm
O_3	7.40	3.76	0.50	0.12
Cl_2	19.8	22.3	25.4	23.6
ClO	10	2[b]	-	-
ClOO	6	3	0.8	-
ClOOCl	37.5	28.6	16.0	12.1
HOCl	9.5	7.8	4.15	2.48
OClO[c]	500	770	600	200
air	1.40×10^{-6}	1.31×10^{-6}	1.11×10^{-6}	1.00×10^{-6}
Model I 0.1μm particle	2.62×10^{9}	2.23×10^{9}	2.09×10^{9}	1.59×10^{9}
Model II 1.0μm particle	1.05×10^{12}	1.07×10^{12}	1.16×10^{12}	1.19×10^{12}
Model III[d] 0.056μm particle 1.0μm particle 3.6μm particle	4.95×10^{6} 2.47×10^{12} 4.32×10^{13}	4.48×10^{6} 2.46×10^{12} 4.38×10^{13}	4.01×10^{6} 2.45×10^{12} 4.45×10^{13}	3.54×10^{6} 2.43×10^{12} 4.52×10^{13}

[a] Cross sections for species other than particles are from DeMore et al [1992].

[b] Difficult estimate because of structured spectrum.

[c] The OClO spectrum is highly structured. Reported cross sections reflect estimation based on TOMS spectral resolution of 1.0 nm.

[d] Cross sections for log normal particle distributions were determined from tables in Beiting (1994a,b).

TECHNOLOGY OPERATIONS

The Aerospace Corporation functions as an "architect-engineer" for national security programs, specializing in advanced military space systems. The Corporation's Technology Operations supports the effective and timely development and operation of national security systems through scientific research and the application of advanced technology. Vital to the success of the Corporation is the technical staff's wide-ranging expertise and its ability to stay abreast of new technological developments and program support issues associated with rapidly evolving space systems. Contributing capabilities are provided by these individual Technology Centers:

Electronics Technology Center: Microelectronics, VLSI reliability, failure analysis, solid-state device physics, compound semiconductors, radiation effects, infrared and CCD detector devices, Micro-Electro-Mechanical Systems (MEMS), and data storage and display technologies; lasers and electro-optics, solid state laser design, micro-optics, optical communications, and fiber optic sensors; atomic frequency standards, applied laser spectroscopy, laser chemistry, atmospheric propagation and beam control, LIDAR/LADAR remote sensing; solar cell and array testing and evaluation, battery electrochemistry, battery testing and evaluation.

Mechanics and Materials Technology Center: Evaluation and characterization of new materials: metals, alloys, ceramics, polymers and composites; development and analysis of advanced materials processing and deposition techniques; nondestructive evaluation, component failure analysis and reliability; fracture mechanics and stress corrosion; analysis and evaluation of materials at cryogenic and elevated temperatures; launch vehicle fluid mechanics, heat transfer and flight dynamics; aerothermodynamics; chemical and electric propulsion; environmental chemistry; combustion processes; spacecraft structural mechanics, space environment effects on materials, hardening and vulnerability assessment; contamination, thermal and structural control; lubrication and surface phenomena; microengineering technology and microinstrument development.

Space and Environment Technology Center: Magnetospheric, auroral and cosmic ray physics, wave-particle interactions, magnetospheric plasma waves; atmospheric and ionospheric physics, density and composition of the upper atmosphere, remote sensing using atmospheric radiation; solar physics, infrared astronomy, infrared signature analysis; effects of solar activity, magnetic storms and nuclear explosions on the earth's atmosphere, ionosphere and magnetosphere; effects of electromagnetic and particulate radiations on space systems; space instrumentation; propellant chemistry, chemical dynamics, environmental chemistry, trace detection; atmospheric chemical reactions, atmospheric optics, light scattering, state-specific chemical reactions and radiative signatures of missile plumes, and sensor out-of-field-of-view rejection.